Modeling Effects of AMOC Variations on Carbon Components

Matthew Boling, Andreas Schmittner

Affiliations

Matthew Boling: College of Physical Sciences and Engineering, Brigham Young University, Rexburg, Idaho

Andreas Schmittner: College of Earth, Ocean, and Atmospheric Sciences, Oregon State University, Corvallis, Oregon

Abstract

The Atlantic Meridional Overturning Circulation (AMOC) is an oceanic current that affects carbon distributions in the ocean as indicated by paleoclimate data and modeling studies. However, carbon cycling and cycling of carbon isotopes ($\delta^{13}C$) is complex, and it currently not understood what causes the observed relationships, such as correlations between AMOC, carbon isotopes, and atmospheric CO_2. In this study, we use a climate model of intermediate complexity that includes diagnostic tracers, allowing for a decomposition of carbon and $\delta^{13}C$. Starting from Last Glacial Maximum (LGM) conditions, both positive and negative freshwater fluxes were applied to the Atlantic Ocean, simulating AMOC changes. Total ocean carbon was decomposed into Dissolved Organic Carbon (DOC) and Dissolved Inorganic Carbon (DIC), with DIC further decomposed into preformed and regenerated components. We find that following AMOC changes, carbon components take more than 3500 years to find their new equilibrium. AMOC collapse from 11 Sv to 2-4 Sv leads to a rapid decrease in atmospheric CO_2 by 5 ppm within 700 years caused by an increase in ocean carbon, which is dominated by an increase in regenerated carbon from remineralization of soft-tissue organic matter mainly in the mid-depth Atlantic. This is followed by a slow increase in atmospheric CO_2 by 8 ppm over 2,800 years dominated by a decrease in the preformed ocean carbon over 2,000 years and a decrease of regenerated carbon after that. The decrease in preformed carbon over the first 2,000 years is dominated by changes in saturation carbon, whereas disequilibrium changes are smaller and of opposite sign. A temporary increase in AMOC from 11 Sv to 26 Sv leads to generally the opposite changes than those of a collapse, except that the system returns to its initial state and that preformed changes are dominated by saturation and not by disequilibrium changes. These results help our understanding of how carbon components respond to AMOC changes and may have implications for the interpretation of paleoclimate data.

Introduction

The Atlantic Meridional Overturning Circulation (AMOC) is a system of oceanic currents that moves water around the Atlantic Ocean and beyond. While the AMOC is part of a larger, global system of oceanic currents, it specifically transports warm surface waters from the tropics and Gulf of Mexico north to the northern North Atlantic. There they cool down and sink below the incoming warm waters. This water mass, now known as North Atlantic Deep Water (NADW), flows southwards (McCarthy et al., 2017; also see Fig. 13). As the surface waters of the Atlantic cool down, the heat is released to the atmosphere. This heat is important in the Earth's climate system – for example, consider the cities of Dublin, Ireland, and Seattle, Washington, United States. Both cities share similar distances from the ocean and elevations. However, Dublin, which generally receives the warmer wind coming from the direction of where the Atlantic water vents heat to the atmosphere, experiences an average winter temperature of several degrees warmer than that of Seattle, even though Seattle's latitude is approximately six degrees closer to the equator (McCarthy et al., 2015).

The ocean contains approximately 60 times as much carbon as the atmosphere (DeVries, 2017). While the lithosphere contains many times more carbon than the hydrosphere, the hydrosphere remains the largest repository of carbon that can be easily exchanged with the atmosphere (DeVries, 2017; Khatiwala et al, 2019). Carbon is essential to all forms of life, and carbon-dioxide (CO_2) is a greenhouse gas that helps sustain Earth's climate. As is typical for most gases, the solubility of CO_2 remains an inverse proportionality to the temperature of the ocean, such that the solubility of warmer tropical waters (around 25°C) is less than half that of cooler polar waters (around 0°C). While salinity also affects the solubility (higher salinity resulting in lower solubility), the effect of the relatively low range of salinity found in the ocean is usually much smaller than that of temperature or negligible under most circumstances (DeVries, 2017).

When CO_2 is absorbed by seawater, carbonic acid (H_2CO_3) is formed. The carbonic acid then breaks into carbonate ions (CO_3^{2-}) and bicarbonate ions (HCO_3^-). Together, these make up what is known as Dissolved Inorganic Carbon (DIC). In the ocean, DIC forms gradients, one being a vertical gradient that bears higher DIC concentrations deeper down and lower DIC concentrations near the surface. These gradients come from ocean carbon pumps, mainly the solubility carbon pump and the biological carbon pump (BCP). These carbon pumps influence how much CO_2 is transferred from the atmosphere to the ocean; it is currently thought that a strong carbon pump during the Least Glacial Maximum (LGM) helped invoke low CO_2 levels in the atmosphere during that time (DeVries, 2017). It is thought that without the BCP, current atmospheric CO_2 levels would be around 200 ppm higher than they presently are (Parekh, 2006). Approximately one-third of the DIC vertical gradient is caused by the solubility pump, and the BCP accounts for the remainder (DeVries, 2017). As the surface ocean absorbs CO_2, phytoplankton in the ocean absorb that CO_2, and as part of the photosynthesis process, convert the CO_2 to Dissolved Organic Carbon (DOC). Zooplankton then ingest that DOC, and excrement it in fecal pellets, which sink to the ocean floor relatively rapidly (Sanders et al., 2014). The BCP is a large factor in sequestering carbon from the ocean's surface – per year, the BCP removes approximately 10 Pg of carbon, and holds approximately 1300 Pg of carbon, keeping it from reaching the ocean's surface (Siegel, et al. 2023).

The amount of the ^{13}C isotope is often expressed as a ratio $R=^{13}C/^{12}C$ with respect to the other stable carbon isotope, ^{12}C. The notation is $\delta^{13}C$ ($R=R_{std}-1$), and it's reported in parts per thousand, or permil (‰), where the standard ratio in the denominator is an accepted average ratio. ^{12}C is preferentially taken up by phytoplankton compared to ^{13}C such that organic matter is depleted in $\delta^{13}C$ by about 20 permil. ^{13}C is also fractionated during air-sea gas exchange and it is impacted by the circulation (e.g. Lunch-Stieglitz et al. 1995, Schmittner and Fillman 2024).

Ice cores provide a relatively detailed history of Earth's climate. As snow falls, the bottom layers of snow are compressed, eventually turning to ice and trapping bubbles of air in the ice. Ice cores can be taken, and under a controlled melting environment, the air bubbles can be captured and studied. The longest ice core record covers a range of approximately 800,000 years (Jouzel, 2013). Studying ice cores have determined that during the last ice age, and as the Earth warmed subsequently, there were rapid changes in the atmospheric CO_2 levels and in $\delta^{13}C$ of CO_2 ($\delta^{13}C_{CO2}$). These rapid changes have been connected with variations in AMOC (Ahn and Brook, 2008; Bauska, et al., 2016), prompting the question of how AMOC changes would impact CO_2 and $\delta^{13}C_{CO2}$.

A previous study investigated carbon distributions in the LGM ocean by decomposing DIC into various components, doing so by using additional diagnostic tracers in the UVic climate model (more on the UVic model in the Materials and Methods section) (Khatiwala et al., 2019). Those additional tracers were recently also applied to $\delta^{13}C$ in LGM equilibrium simulations (Schmittner and Fillman, 2024), however what still remained to be studied is applying the model, with the additional tracers, to transient AMOC changes. This research intends to address this gap in understanding.

Materials and Methods

The University of Victoria produced an intermediate complexity climate model that Oregon State University modified (named OSU-UVic), which is a climate model that includes land, ocean, and atmosphere components (Mengis et al. 2020). The oceanic component consists of a three-dimensional grid with a zonal resolution of 3.6°, a meridional resolution of 1.8°, and 19 levels of vertical resolution. To keep the model computationally efficient, the atmosphere component is greatly simplified as a single-layer Energy-Moisture-Balance-Model (Weaver, et al. 2001). The model includes ocean circulation, carbon isotopes, plankton, fluxes of nutrients and elements, and sea ice (Schmittner and Fillman, 2024). Boundary conditions, such as freshwater flux in the ocean can be set, producing useful data to help understand the relationship between AMOC behavior and carbon levels in the ocean and atmosphere.

For this research, two different simulations were performed. The first ("uprun") increased the freshwater flux (FWF) into the ocean at a steady rate for five hundred years, and the second ("downrun") decreased the freshwater flux into the ocean at that same rate for five hundred years, with both runs initially starting at a FWF rate of zero and a data-constrained LGM initial condition (Muglia and Schmnittner, 2021). After the first 500 years, the FWF was set to zero for the remainder of the run.

We decompose the DIC into separate components. The DIC is broken down into its preformed (C_{pre}), soft-tissue (C_{soft}), and Calcium Carbonate ($CaCO_3$) components. The difference between the C_{pre} and the saturated (C_{sat}) components can be referred to as the disequilibrium (C_{dis}) component, or in other words, $C_{pre} - C_{sat} = C_{dis}$. This equation can be rewritten as $C_{pre} = C_{sat} + C_{dis}$, effectively breaking down the C_{pre} into C_{sat} and C_{dis} components. This method was used in the model to track the difference between the C_{pre} and the C_{sat}.

Results

In previous studies, it was commonly found that increasing the FWF led to a reduction or a full collapse of AMOC (Ivanovic et al., 2017; Weijger et al., 2019, Wood et al., 2019). This is consistent with my model run (Fig. 1B). After the AMOC collapse from an initial 11 Sverdrups (Sv; 1 Sv = $10^6 m^3/s$) to a peak low of about 2 Sv, it regains a little bit of strength, back up to a little over 4 Sv by model year 3500, appearing to eventually come to an equilibrium around there. This is in contrast to the downrun, with the decreasing FWF (Fig. 2). The AMOC starts at the same 11 Sv, peaks at about 26 Sv, then once the FWF goes to zero, the AMOC strength very quickly drops, eventually coming to equilibrium at the same strength that it started out as.

In figure. 1C, the total amount of carbon in the atmosphere, ocean, and land components are broken down. While the FWF is cut off at year 500, and AMOC starts to regain strength around that same time, the peaks/dips of the amount of carbon are delayed by roughly 300 years, peaking around model year 800. Compare that to figure 2C, where the carbon in the atmosphere, ocean, and land components peak a little bit earlier, somewhere between model years 600 and 700. The peaks in the downrun are earlier presumably because the AMOC returns more quickly to its initial condition to the uprun where the AMOC changes are slower after year 500.

CO_2 in the atmosphere (Fig. 1D) reaches a low around model year 700, then goes back up, higher than where it started and it continues to climb by the model year 3500. While the downrun is closer to equilibrium at year 3500, the total range of the atmospheric CO_2 change within these 3500 years is approximately 8 ppm (parts per million) in both uprun and downrun (figure 2D). The $\delta^{13}C$ in both runs (Figs. 1E and 2E) reach their respective max/min around year 500, with similar ranges of 0.12-0.14 ‰. Figures 1F and 2F show the oceanic $\delta^{13}C$. Both have similar ranges of 0.4-0.5‰ and both reach their respective min/max shortly before year 700. These results imply that the changes in atmospheric CO_2 and $\delta^{13}C_{CO2}$ are caused by changes in ocean carbon and $\delta^{13}C$, respectively.

Figures 3 and 4 break down the total oceanic carbon by ocean basin, with figure 3 being the results from the uprun, and figure 4 being the results from the downrun. In each figure, panel A shows the total oceanic carbon, while panels B, C, and D break that down into the Atlantic, Pacific, and Indian oceans, respectively, with all totals being given in petagrams. First off, note that the Pacific is the largest ocean basin, containing roughly half of the total carbon (see figures 3A and 3C). While it may initially seem that the Pacific would therefore be the main controlling factor in the behavior of the total amount of carbon in the global ocean, this is not the case. Comparing figure 4A to 4C, the behavior of

the total carbon is not even remotely close to that of the Pacific – it follows the Atlantic much more closely. This is due to the change being greatest in the Atlantic.

Something else to note in figure 4 is the carbon in the Indian ocean. It initially goes up for the first ~400 years, imitating the Pacific, but then the amount of carbon drops like the Atlantic does. This is likely due to the fact that the carbon-rich waters of the Pacific reach the Indian ocean first, but then the carbon-deficit waters of the Atlantic reach the Indian ocean at about the same time that the carbon level in the Pacific starts to drop (also see figure 13). This results in a rapid drop of carbon levels in the Indian ocean, until about year 750. At that point, the carbon levels in the Atlantic have been increasing for a while, and subsequently re-nourish the Indian with carbon. This is explored more in figures 11 and 12.

Figures 5 and 6 look at the global-average concentrations of DIC and DOC, and also their respective ratios $\delta^{13}C$. First off, note that there is much more DIC than DOC (panels A and C, respectively), by a factor of roughly 800. Another thing of note here is that in panel C of both figures, the DOC responds much more rapidly than the DIC does (panel A), finding its equilibrium roughly by year 1000 (figure 5C) or year 1500 (figure 6C), as opposed to the DIC, which is still changing appreciably by model year 3500. DOC responds more quickly because it is confined mainly to the upper ocean where it is produced, whereas DIC is relatively more abundant in the deep ocean and thus responds slower. There is also a significant difference between how much the concentration of DOC changes – in the uprun (figure 5C), the DOC levels have a total range of about $2.5\ 10^{-4}$ mol/m^3, whereas the downrun (figure 6C) changes by $7\ 10^{-5}$ mol/m^3, only about 1/3 of that of the uprun.

Panel D in figure 5 shows the globally-averaged $\delta^{13}C$. The ratio remains relatively constant for approximately the first 250 years, rises until around model year 1000, then falls again, ending up slightly below its initial equilibrium by model year 3500. One possibility for this behavior is that the surface ocean $\delta^{13}C$ follows the atmospheric $\delta^{13}C_{CO2}$, which shows this behavior. Further analysis of the surface ocean $\delta^{13}C_{DIC}$ is needed to fully answer this question.

Figures 7 (uprun) and 8 (downrun) take the global DIC (panel A), and break it down into its three components – preformed DIC (DIC_{pre}), soft-tissue DIC (DIC_{soft}), and calcium carbonate ($CaCO_3$), in panels B, C, and D, respectively. While the C_{pre} comprises most of the total DIC, the change in C_{pre} is less than that of the combined change of C_{soft} and $CaCO_3$, with the latter two following very similarly shaped curves. Hence, in both uprun and downrun, the total DIC follows the behavior of the combination of C_{soft} and $CaCO_3$.

Figures 9 and 10 take the C_{pre} (panel A) and break it down into its saturated (C_{sat}, panel B) and disequilibrium (C_{dis}, panel C) components. Note that in the uprun (figure 9), the C_{sat} is the controlling factor of the total C_{pre}, whereas in the downrun (figure 10), the C_{pre} follows much more closely the behavior of the C_{dis}.

Figures 11 (uprun) and 12 (downrun) model longitudinally averaged concentrations of DIC in the three ocean basins in figures 3 and 4. Recall in figure 4D, that the amount of DIC in the Indian ocean spiked around 400 years, then dropped until about year 750, then went up after that. The model years in figures 11 and 12 were chosen to further analyze that behavior of DIC in the Indian ocean.

In figure 11, while the Pacific doesn't appear to change much from year 0 to 700, there are changes going on in the other two ocean basins. The presence of the carbon-deficit North Atlantic Deep Water (NADW) is evident in the upper-right of panel A of figure 11, and the contour lines that are horizontal for most of the figure, but then drop vertical at low latitudes between 1 and 2 km depth, then return horizontal again ,signify the presence of a healthy AMOC, recalling from figure 1B that at year 0, the AMOC strength was 11 Sv. Moving down to panel B, year 400, AMOC has collapsed at this point (figure 1B) indicated by the lack of the stair-step contour lines and higher DIC levels in the North Atlantic between about 1-2 km depth. Panel C is only three hundred years later; however, the accumulation of carbon in the middle and deeper depths of the North Atlantic is starting to become evident. By year 3500 (panel D), there is a large intrusion of carbon-rich water in the north Atlantic, much of it coming from the Pacific (panel L).

Throughout this whole ordeal, the Indian doesn't change much. From panel E (0 yr) to panel F (400 yr), then to panel G (700 yr), it's hard to tell what the overall DIC amount is doing; however, referring back to figure 3D, and recalling that the amount of DOC is insignificant to the amount of DIC (by a factor of about 800), the DIC level in the Indian lowers throughout all four panels in figure 11.

Examining the behavior of the Pacific, there is little to no change in the DIC distribution for panels I, J, and K. The only significant change shows up in panel L (year 3500), when the highest concentration of DIC in the northern part disappears and shows up in the northern part of the Atlantic.

In figure 12, note that the top row of panels, year 0, is the same as that of figure 11. Recall that the downrun had the negative FWF, resulting in the high AMOC strength, spiking from 11 Sv to 26 Sv. This is evident in comparing the contour lines of B to that of A. In panel A, the stair-step contour lines signify a healthy AMOC, whereas in panels B and C, those "stair-steps" have turned into s-shaped curves, indicating a much stronger AMOC, consistent with figure 2B, with lower DIC at mid depth in the North Atlantic. By 3500 yr, the AMOC strength (figure 2B) and the resulting DIC distribution (figure 12D) have returned close to what they were at year 0.

Enhanced advection of low DIC NADW into the Indian ocean seems to lower DIC concentrations there at mid depth by the year 700, consistent with Fig. 4D. Subsequently, DIC concentrations in the Indian ocean return to their initial values.

There is very little change apparent in the Pacific. Despite the fact that the total carbon is changing some (figure 4C), this change is small enough compared to the vastness of the Pacific ocean that it can't be seen here in figure 12. To more easily visualize the changes in the Pacific ocean, plotting differences between the initial state and each respective year might prove to be useful.

Discussion

This research has provided insight into the behavior of different components of carbon and its isotopes as a response to AMOC changes, using diagnostic tracers. In general, in the uprun where AMOC collapsed, the various carbon components reacted in their respective ways, eventually approaching some equilibrium that is different from their initial starting value. In contrast, in the

downrun where AMOC strengthened briefly but then settled back down to its initial value (figure 2B), the various carbon components initially react with the opposite sign as to the uprun, but unlike the uprun, they then approach roughly their initial equilibrium value.

While for most quantities the changes in the downrun, representing an AMOC increase, were opposite to those in the uprun, representing an AMOC collapse, differences were seen in the breakdown of DIC_{pre} into DIC_{sat} and DIC_{dis}. In the downrun, DIC_{dis} is the controlling factor of the total change in DIC_{pre}, whereas in the uprun, the DIC_{sat} is the controlling factor (note that in each figure, the respective other component has a change of the opposite sign). This is different from a previous study of LGM minus Pre-Industrial equilibrium changes, where DIC_{dis} was found to be the controlling factor (Schmittner and Fillman, 2024), suggesting that different carbon components can dominate depending on the forcing (transient AMOC vs LGM equilibrium).

Conclusion

Understanding the behavior of the different components of the ocean carbon is vital to understanding Earth's climate, and this study examined the behavior of different carbon isotopes and components in response to changes in AMOC strength. One limitation of this study was simply time; in the allocated time for this research, there simply wasn't enough time to allow the models to run for significantly longer. For instance, the C_{dis} in figure 9C is still changing rapidly by model year 3500, and it could prove advantageous to allow these models to run further to see how these carbon components behave.

Acknowledgments

I would like to thank the National Science Foundation for funding my research. I'd also like to thank Mia El-Khazen and Schmitty Thompson for their time spent answering my questions and helping me when I got stuck, and Kaplan Yalcin and Kelsey Lane for running this REU program.

References

Ahn, J., and Brook, E. (2008)
Atmospheric CO2 and Climate on Millennial Time Scales During the Last Glacial Period
Science 322, 83-85, DOI:10.1126/science.1160832

Bauska, T., Baggenstos, D., Brook, E., Mix, A., Marcott, S., Petrenko, V., Schaefer, H., Severinghaus, J., and Lee, J. (2016)
Carbon isotopes characterize rapid changes in atmospheric carbon dioxide during the last deglaciation
PNAS, 113, 13, 3465-3470, doi:10.1073/pnas.1513868113

DeVries, T (2022)
The Ocean Carbon Cycle
Annual Review of Environment and Resources, vol 47, pg 317-341, https://doi.org/10.1146/annurev-environ-120920-111307

Ivanovic, R. F., L. J. Gregoire, A. D. Wickert, P. J. Valdes, and A. Burke (2017)
Collapse of the North American ice saddle 14,500 years ago caused widespread cooling and reduced ocean overturning circulation
Geophys. Res. Lett., 44, 383–392, doi:10.1002/2016GL071849

Jouzel, J. (2013)
A brief history of ice core science over the last 50 yr
Clim. Past, 9, 2525–2547, https://doi.org/10.5194/cp-9-2525-2013, 2013.

Khatiwala, S., Schmittner, A., Muglia, J. (2019)
Air-sea disequilibrium enhances ocean carbon storage during glacial periods
Science Advances, DOI: 10.1126/sciadv.aaw4981

McCarthy, G.D., Gleeson, E., and Walsh, S. (2015)
The influence of ocean variations on the climate of Ireland
Weather 70, 242-245

McCarthy, G.D., Smeed, D.A., Cunningham, S.A. and Roberts, C.D. (2017)
Atlantic Meridional Overturning Circulation.
MCCIP Science Review 2017, 15 - 21. doi:10.14465/2017.arc10.002-atl

Mengis, N., Keller, D. P., MacDougall, A. H., Eby, M., Wright, N., Meissner, K. J., Oschlies, A., Schmittner, A., MacIsaac, A. J., Matthews, H. D., and Zickfeld, K. (2020)
Evaluation of the University of Victoria Earth System Climate Model version 2.10 (UVic ESCM 2.10)
Geosci. Model Dev., 13, 4183–4204, https://doi.org/10.5194/gmd-13-4183-2020

Muglia, J., and Schmittner, A. (2021)
Carbon Isotope Constraints on Glacial Atlantic Meridional Overturning: Strength vs Depth
Quaternary Science Reviews, 257, 106844, doi: 10.1016/j.quascirev.2021.106844

Parekh, P., S. Dutkiewicz, M. J. Follows, and T. Ito (2006)
Atmospheric carbon dioxide in a less dusty world

Geophys. Res. Lett., 33, L03610, doi:10.1029/2005GL025098

Sanders, R., Henson, S., Koski, M., De La Rocha, C., Painter, S., Poulton, A, Riley, J., Salihoglu, B., Visser, A., Yool, A., Bellerby, R., and Martin, A. (2014)
The Biological Carbon Pump in the North Atlantic
Progress in Oceanography, 129B, 200-218, https://doi.org/10.1016/j.pocean.2014.05.005.

Schmittner, A., & Fillman, N. J. (2024)
Carbon and carbon-13 in the preindustrial and glacial ocean
PLOS Climate, 3(7), e0000434. doi: 10.1371/journal.pclm.0000434

Siegel, D., DeVries, T., Cetinić, I., Bisson, K. (2023)
Quantifying the Ocean's Biological Pump and Its Carbon Cycle Impacts on Global Scales
Annual Review of Marine Science, 15:329-56, https://doi.org/10.1146/annurev-marine-040722-115226

Weaver, A., Eby, M., Wiebe, E., Bitz, C., Duffy, P., Ewen, T., Fanning, A., Holland, M., MacFadyen, A., Matthews, H., Meissner, K., Saenko, O., Schmittner, A., Wang, H., and Yoshimori, M. (2001)
The UVic earth system climate model: Model description, climatology, and applications to past, present and future climates
Atmosphere-Ocean, 39:4, 361-428, DOI: 10.1080/07055900.2001.9649686

Weijer, W., Cheng, W., Drijfhout, S. S., Federov, A.V., Hu, A., Jackson, L. C., et al. (2019)
Stability of the Atlantic Meridional Overturning Circulation: A review and synthesis.
Journal of Geophysical Research: Oceans, 124, 5336–5375. https://doi.org/10.1029/2019JC015083

Wood, R.A., Rodríguez, J.M., Smith, R.S. *et al.*
Observable, low-order dynamical controls on thresholds of the Atlantic meridional overturning circulation.
Clim Dyn **53**, 6815–6834 (2019). https://doi.org/10.1007/s00382-019-04956-1

Figures and Tables

Figure 1

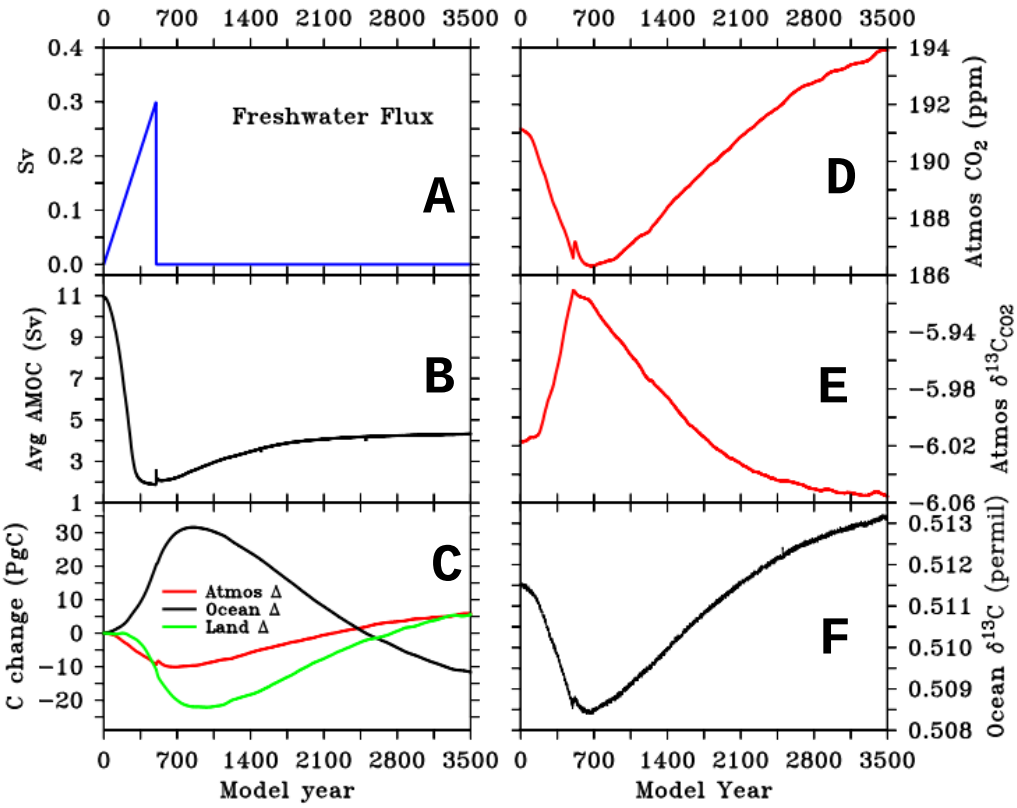

Figure 1:
Panel **A** shows the Freshwater Flux (FWF) in Sverdrups (Sv). The flux is increasing at a steady rate of $6x10^{-4}$Sv/yr for the first 500 years, maximizing at 0.3 Sv. Then the FWF is cut off, and remains at zero Sv for the remaining 3000 years.
Panel **B** shows the average strength of the AMOC in Sv.
Panel **C** shows the total carbon change in the atmosphere (red), ocean (black), and land (green).
Panel **D** shows the globally averaged CO_2 concentration in parts per million in the atmosphere.
Panel **E** shows the $\delta^{13}C_{CO2}$ in the atmosphere.
Panel **F** shows the $\delta^{13}C$ in the ocean in permil (parts per million).

Figure 2

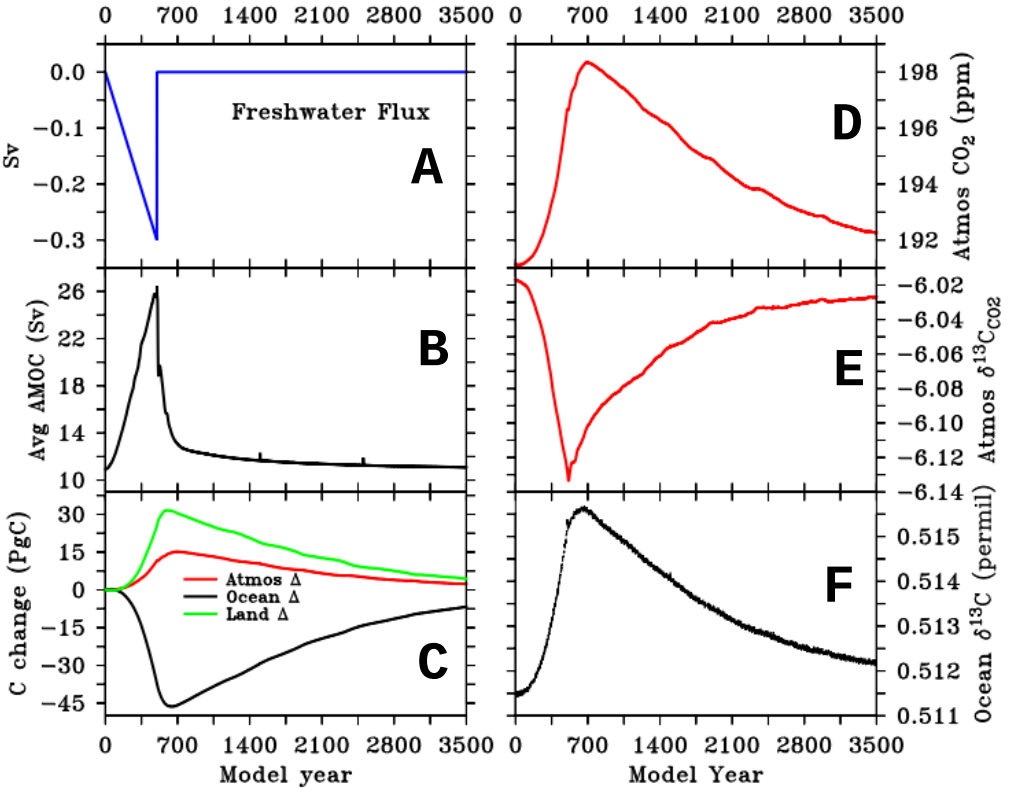

Figure 2:
As figure 1, but in panel **A** the FWF is decreasing at a steady rate of $-6x10^{-4}$Sv/yr for the first 500 years, reaching a peak at -0.3 Sv. Then the FWF returns to zero for the remaining 3000 years.

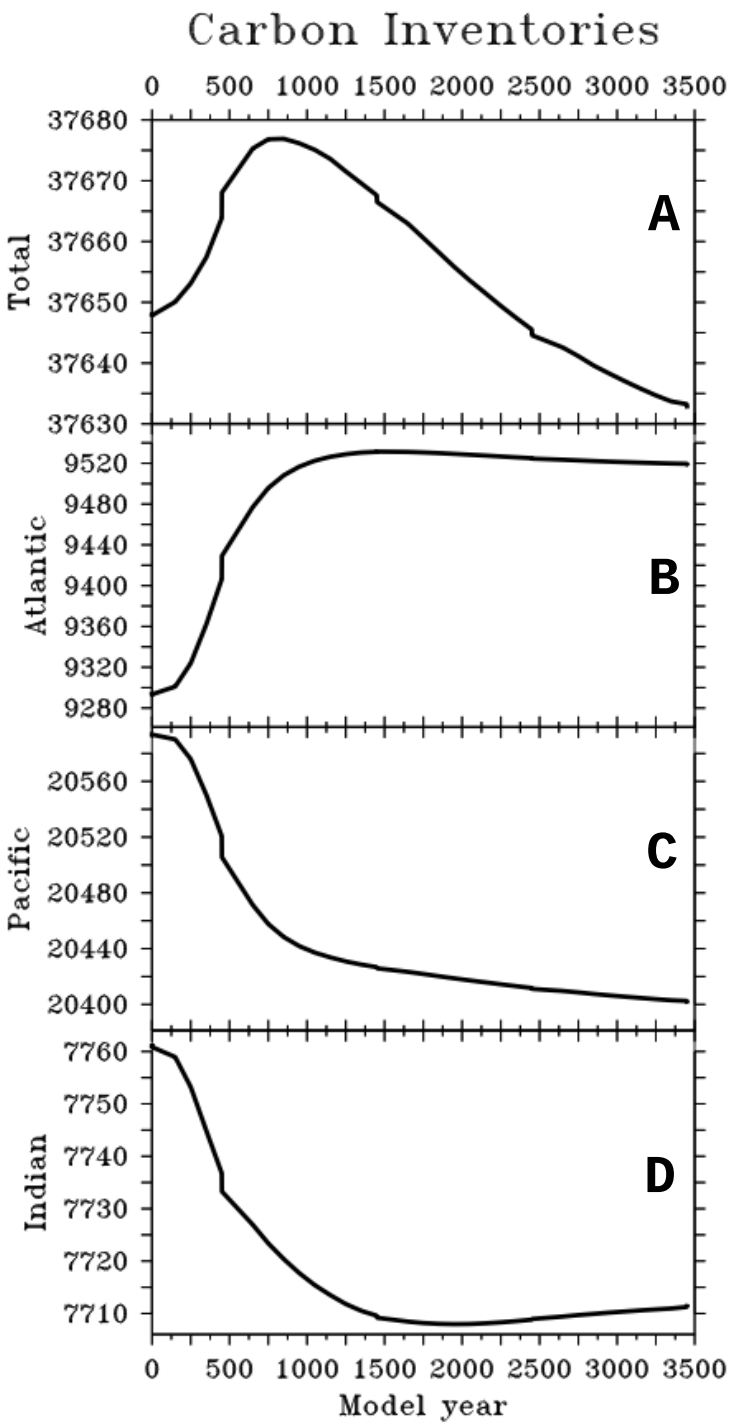

Figure 3

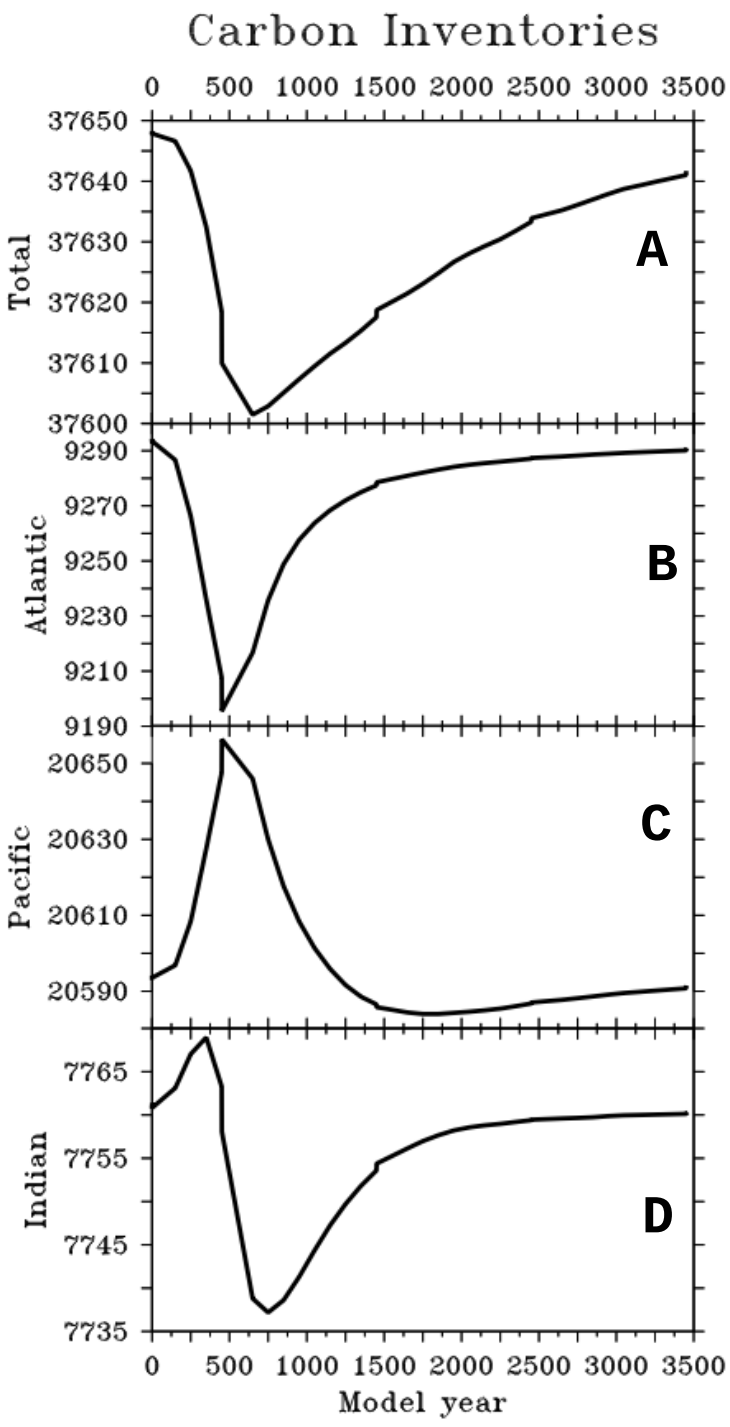

Figure 4

Figure 3: Panel **A** shows the total carbon in the global ocean as the freshwater flux (FWF) is increased (uprun), making AMOC change. Panels **B**, **C**, and **D** show the breakdown of that carbon in the Atlantic, Pacific, and Indian ocean basins, respectively. All vertical axis scales are in Petagrams.

Figure 4: As figure 3, except the FWF is decreasing (downrun).

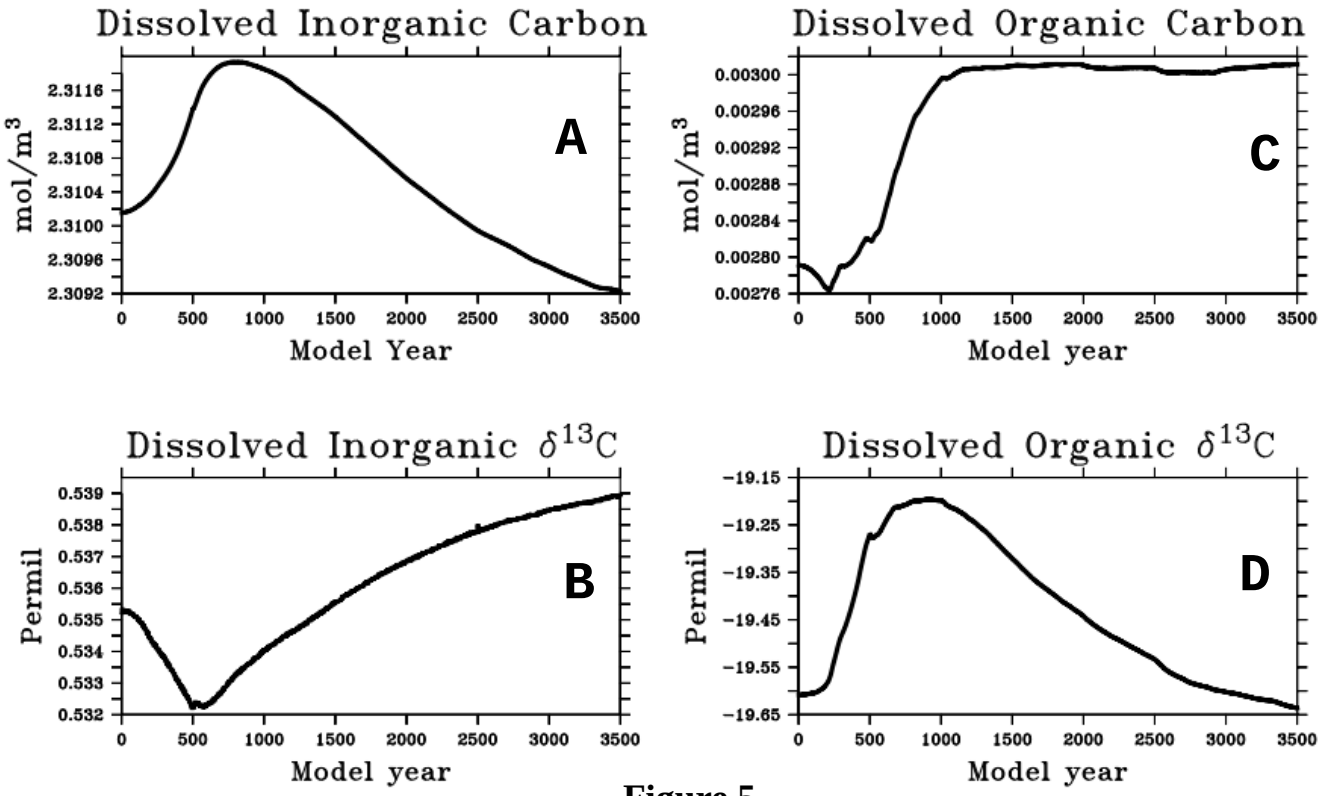

Figure 5

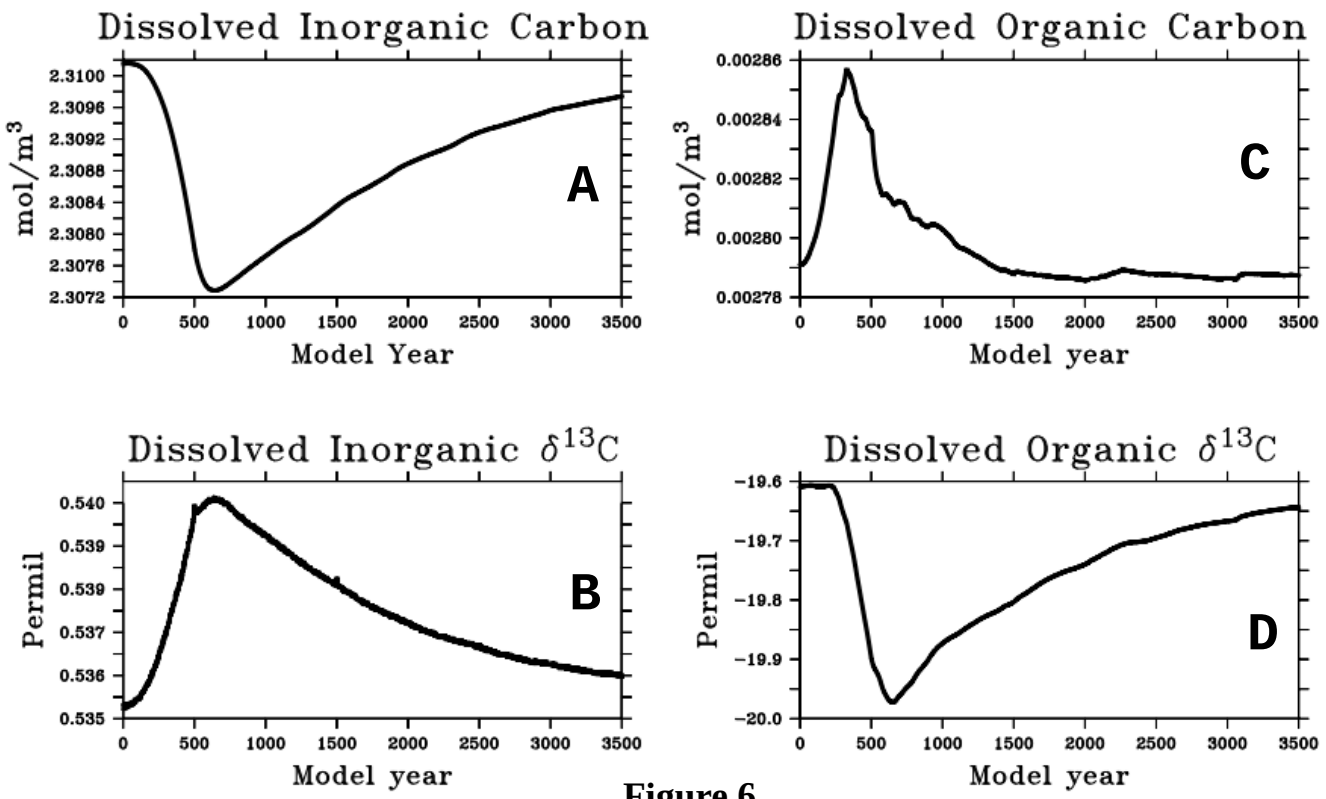

Figure 6

Figure 5: Shows the behavior of the Dissolved Inorganic Carbon (DIC) and Dissolved Organic Carbon (DOC) as the Atlantic Meridional Overturning Circulation increases from the increasing Freshwater Flux (FWF). Panel **A** shows the concentration of DIC in moles of DIC per cubic meter of ocean water, Panel **B** shows the carbon isotope ratio of the DIC. Panel **C** shows the concentration of DOC in moles of DOC per cubic meter of ocean water, and Panel **D** shows the carbon isotope ratio of the DOC.

Figure 6: As figure 5, except a decreasing FWF is applied (downrun).

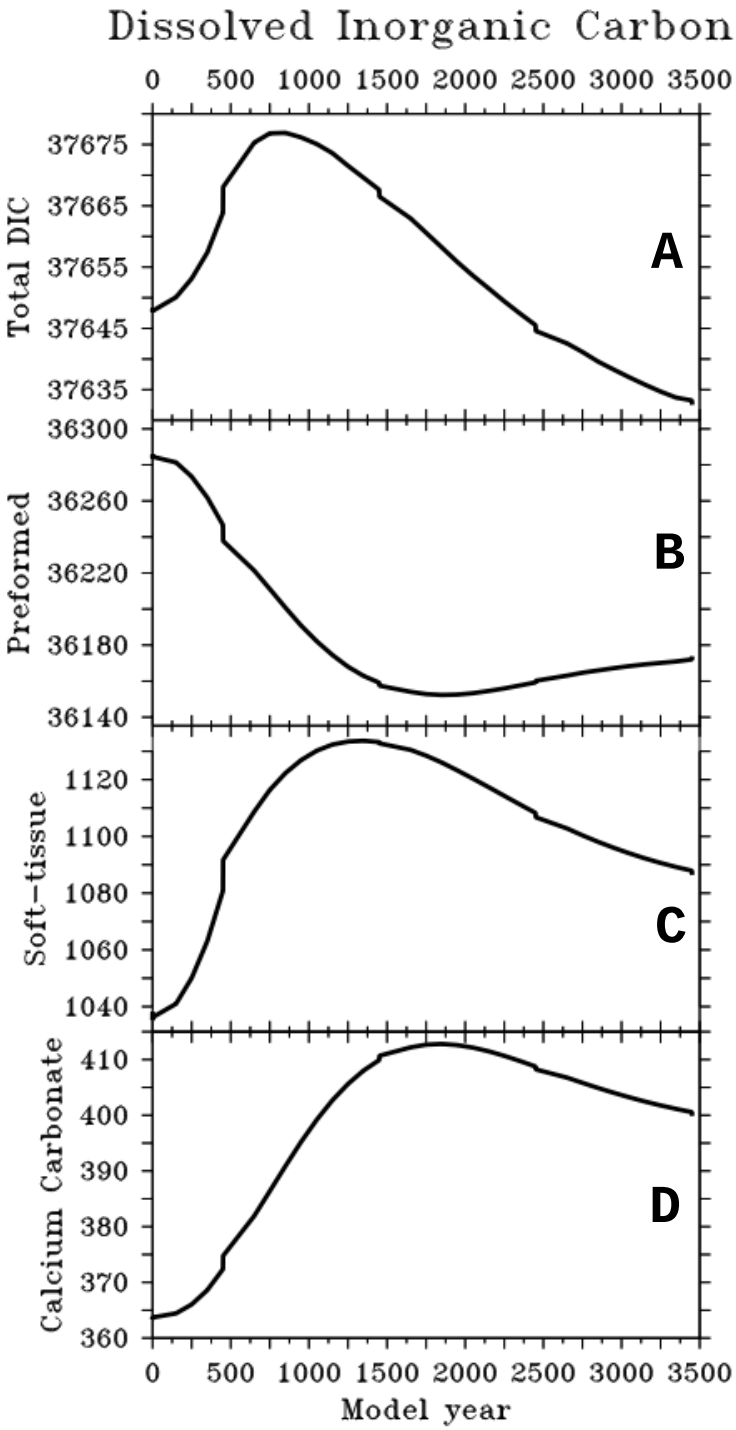

Figure 7

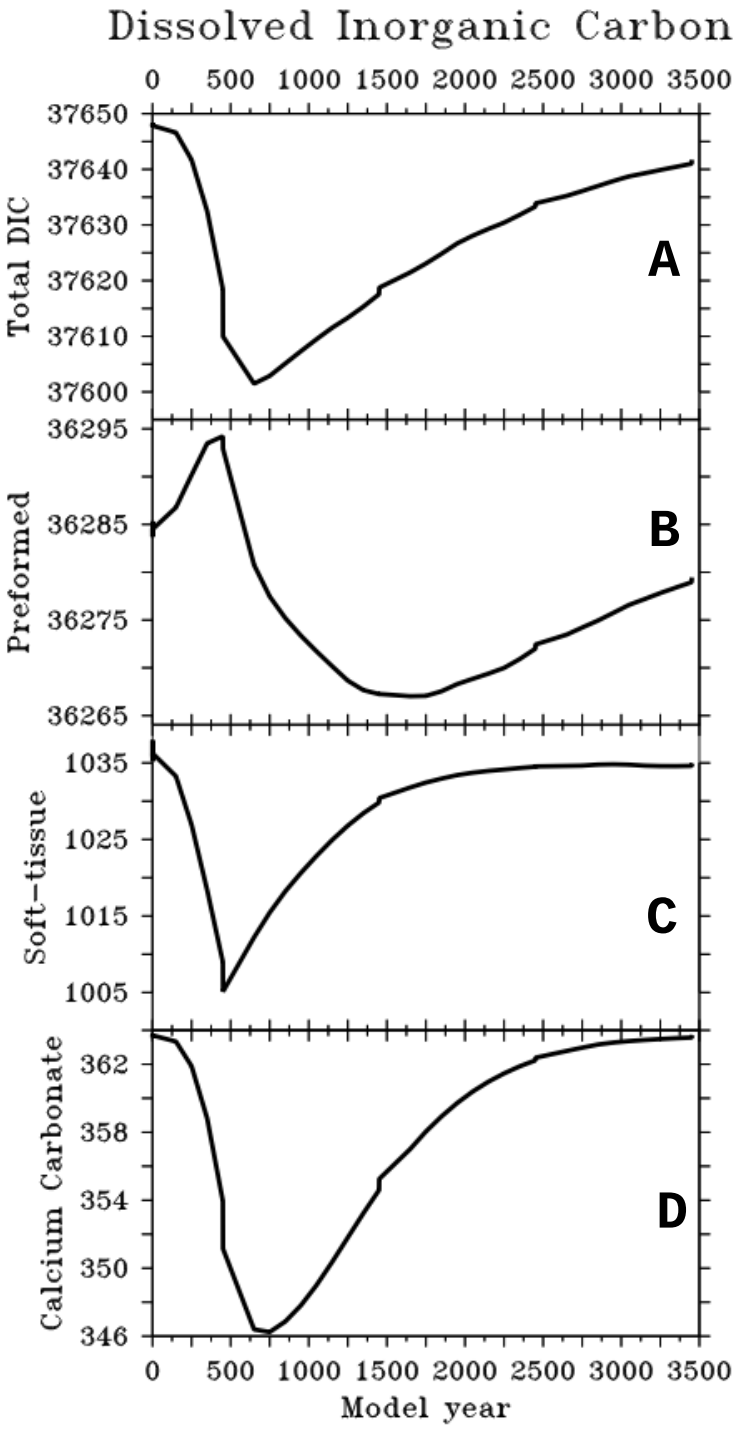

Figure 8

Figure 7: The total DIC in the global ocean is broken down into its various components. Panel **A** shows the total DIC as the FWF is increased (uprun), panel **B** shows the amount of preformed carbon, panel **C** shows the amount of soft-tissue carbon, and panel **D** shows the amount of Calcium Carbonate. All vertical axis scales are in Petagrams.

Figure 8: As figure 7, except a decreasing FWF is applied (downrun).

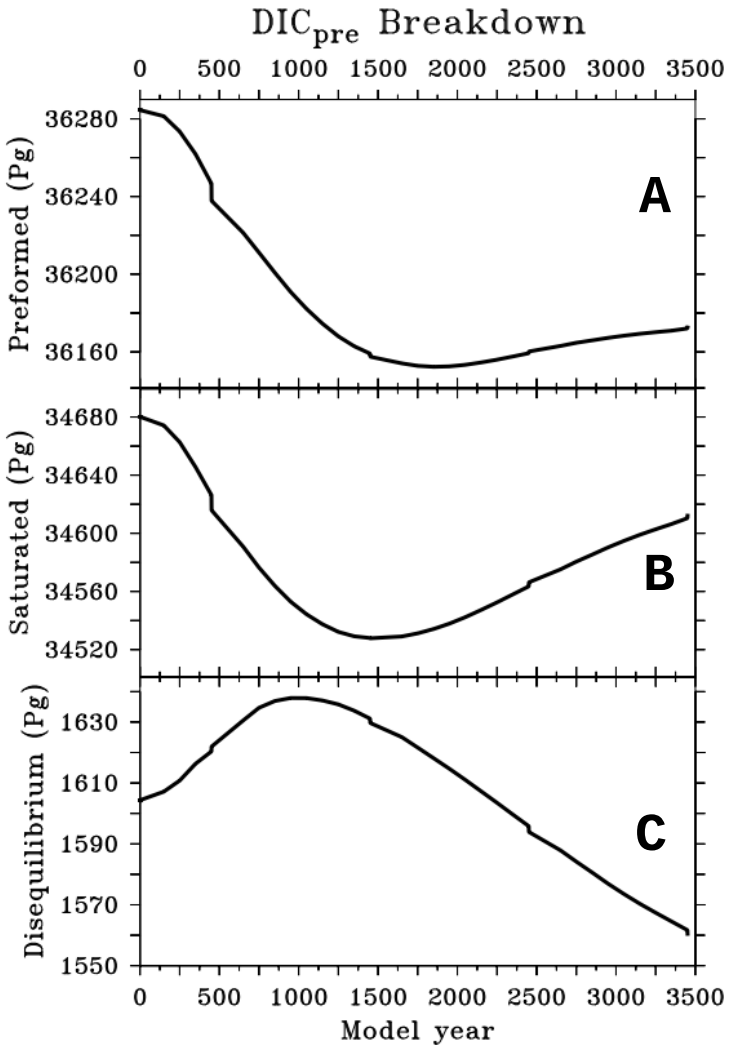

Figure 9

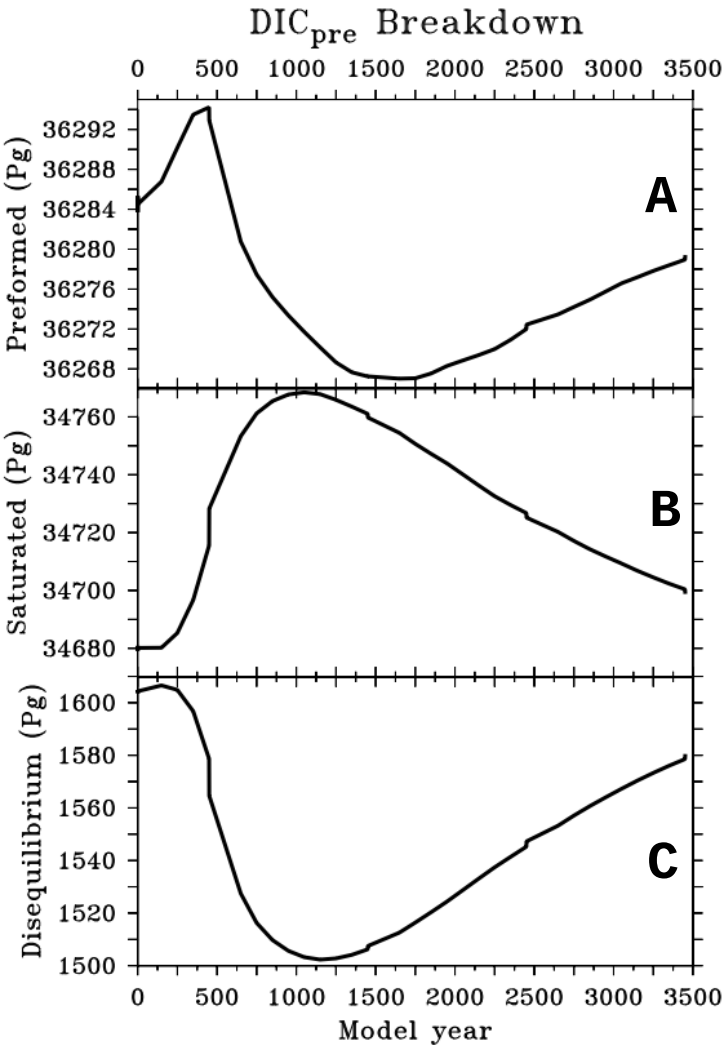

Figure 10

Figure 9: The Preformed Dissolved Organic Carbon (DIC_{pre}) is broken down into its individual components – Saturated carbon (C_{sat}) and Disequilibrium carbon (C_{dis}). Panel **A** shows total DIC_{pre}, and panels **B** and **C** break it down into it's C_{sat} and C_{dis} components, respectively, as the FWF increases (uprun).

Figure 10: As figure 9, except a decreasing FWF is applied (downrun).

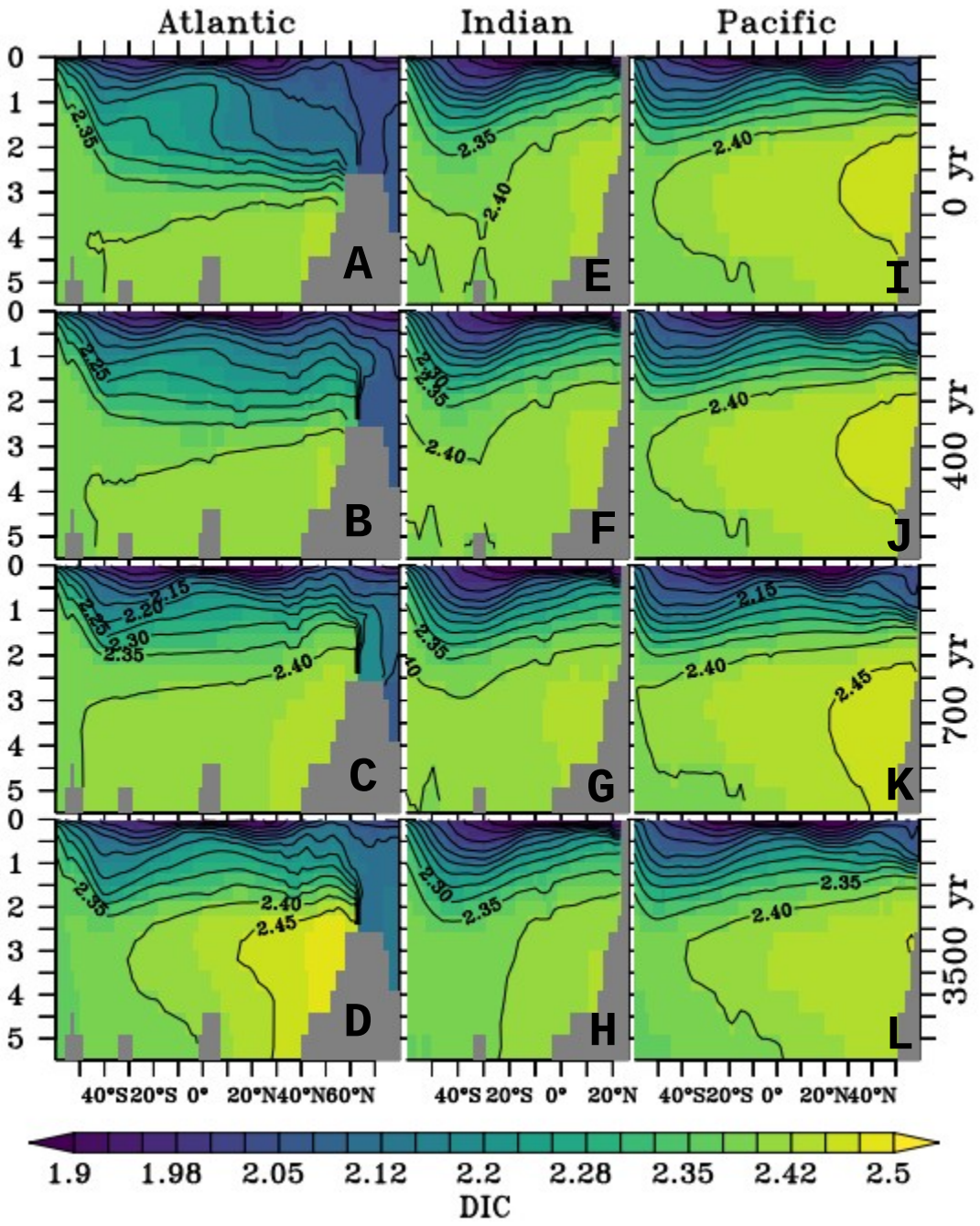

Figure 11

Figure 11 shows longitudinally averaged densities of Dissolved Inorganic Carbon in the Atlantic, Indian, and Pacific ocean basins, at model years 0, 400, 700, and 3500, based on the increasing FWF (uprun). The depth in kilometers is on the vertical axis, and the latitude in degrees is on the horizontal axis. The density is in moles of DIC per cubic meter of ocean water.

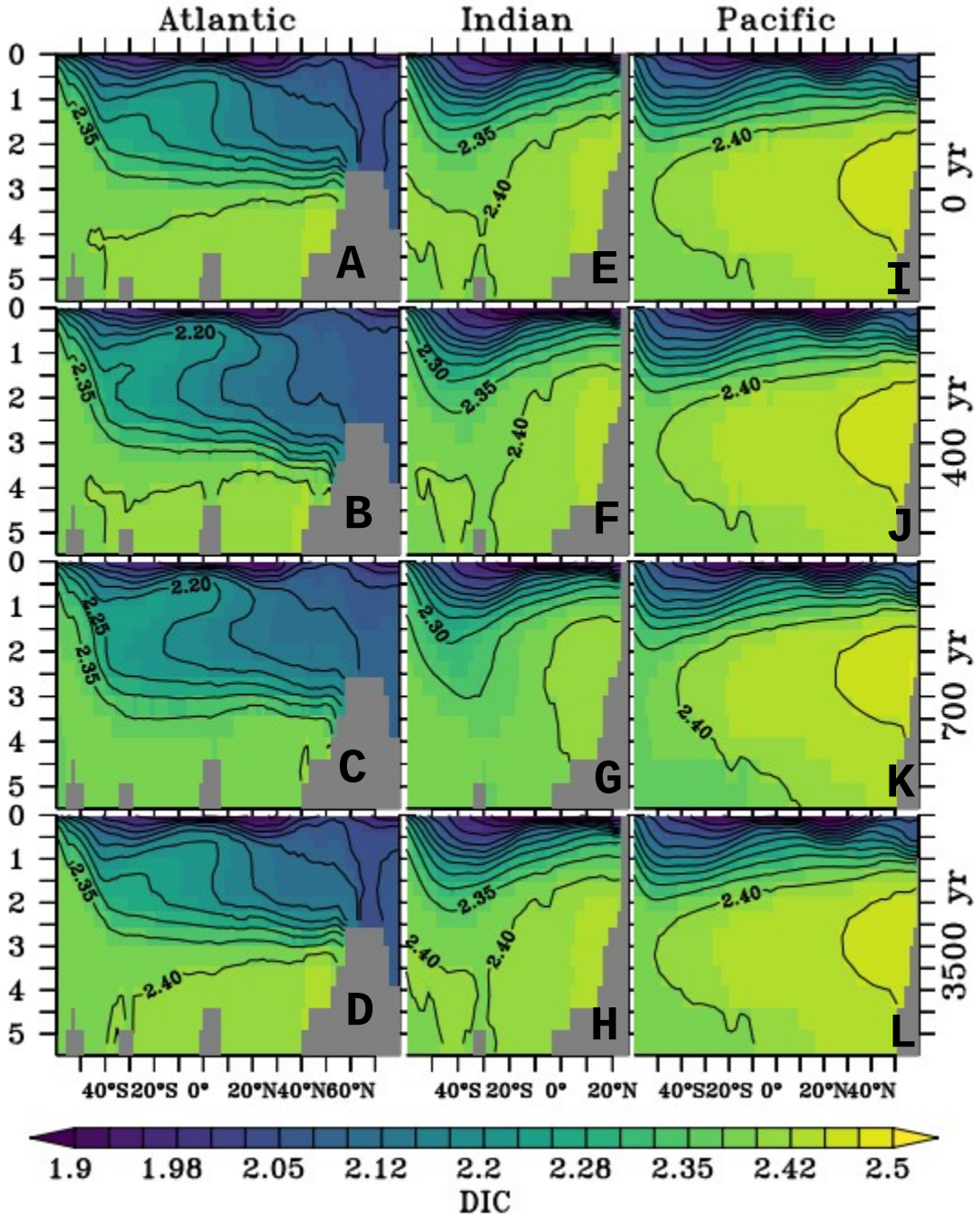

Figure 12

Figure 12: As figure 11, except a decreasing FWF is applied (downrun).

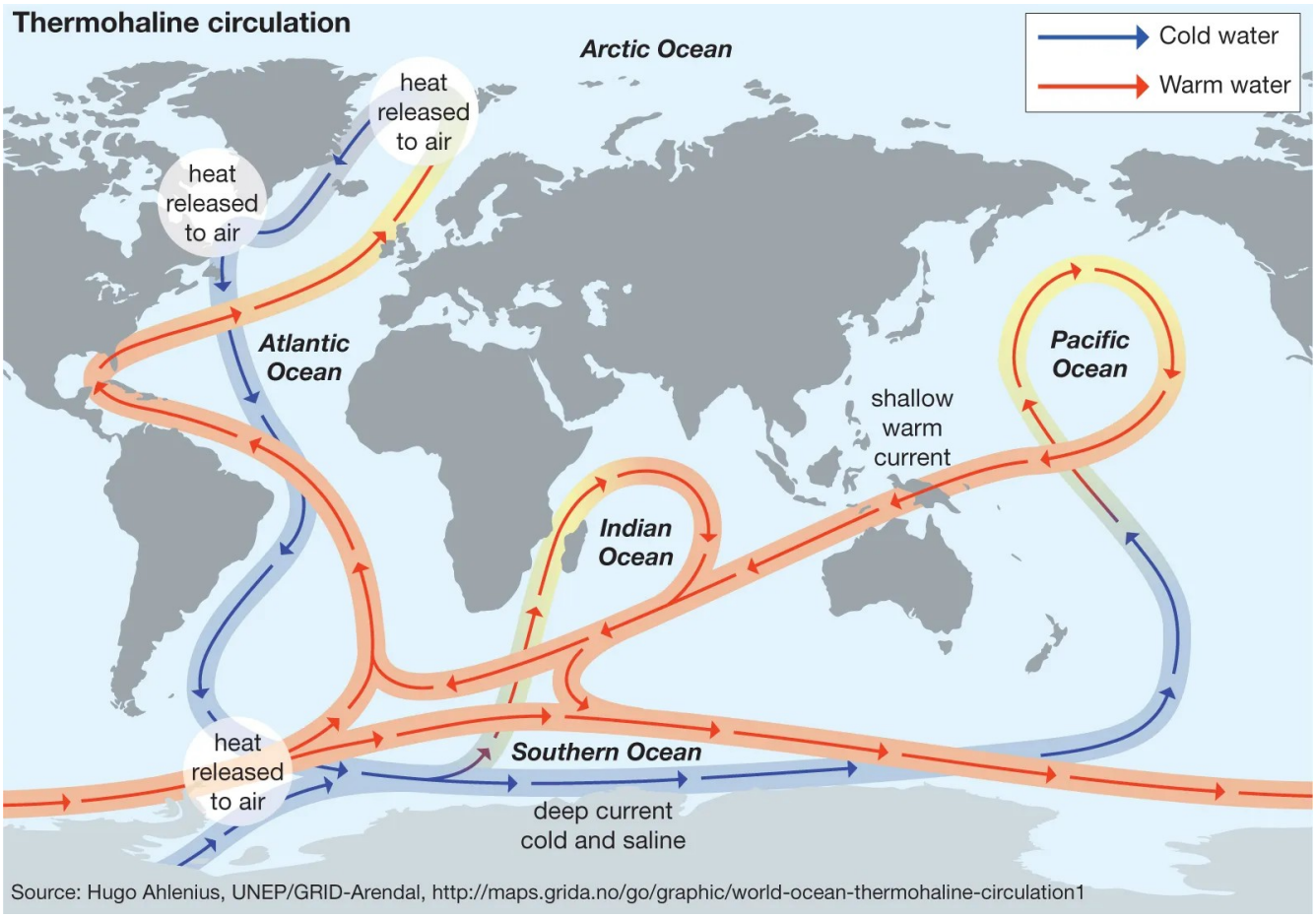

Figure 13

Figure 13 shows the thermohaline circulation. Arrows indicate direction of water transport, while color represents water temperature (see figure for legend).